IEEE Photonics Journal
An IEEE Photonics Society Publication

Open Access

Fiber Nonlinearity and Tight Filtering Impairments Mitigation of DP-16QAM Nyquist-WDM Systems Using Multiplier-Free MAP Detection

Volume 11, Number 6, December 2019

Tao Yang
Chen Shi
Liqian Wang
Xue Chen
Haoyuan Pan
Huan Chen
Min Zhang
Zhiguo Zhang

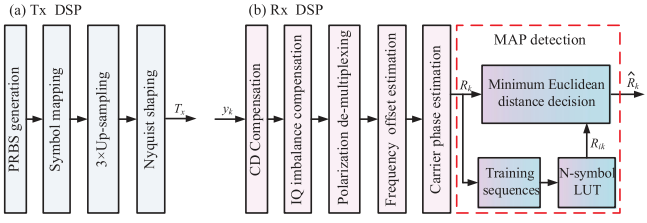

DOI: 10.1109/JPHOT.2019.2947459

Fiber Nonlinearity and Tight Filtering Impairments Mitigation of DP-16QAM Nyquist-WDM Systems Using Multiplier-Free MAP Detection

Tao Yang,[1] **Chen Shi**,[2] **Liqian Wang**,[1] **Xue Chen**,[1] **Haoyuan Pan**,[1] **Huan Chen**,[1] **Min Zhang**,[1] **and Zhiguo Zhang**[1]

[1]State Key Laboratory of Information Photonics and Optical Communications, Beijing University of Posts and Telecommunications, Beijing 100876, China
[2]Department of Electrical and Computer Engineering, Iowa State University, Ames, IA 50011 USA

DOI:10.1109/JPHOT.2019.2947459

Manuscript received July 29, 2019; revised October 7, 2019; accepted October 11, 2019. Date of publication October 15, 2019; date of current version November 12, 2019. This work was supported by the National Natural Science Foundation of China under Grant 61571061. Corresponding author: Xue Chen (e-mail: xuechen@bupt.edu.cn).

Abstract: Tight filtering and fiber Kerr effect both cause severe pattern-dependent distortions that need to be combated to achieve higher spectral efficiency (SE), larger capacity and greater achievable transmission distance in the next generation wavelength division multiplex (WDM) optical transmission system. In this paper, a novel multiplier-free maximum-a-posteriori-probability (MAP) detection scheme is proposed and verified in dual-polarization (DP) 16-ary quadrature amplitude modulation (16-QAM) Nyquist-WDM systems. Based on the innovative technique of approximate calculation of Euclidean distance, the competitive performance is obtained in terms of pattern-dependent impairments mitigation. Besides, the computational complexity (CC) is drastically reduced to about 34%, as the multiplier of the proposed MAP detection is completely removed. Comprehensive simulation results of triple-carrier Nyquist DP 16-QAM demonstrate that the MAP scheme could effectively mitigate the tight filtering and fiber nonlinearity impairments with much lower CC, i.e., achieve desirable SE and nonlinearity tolerance in long-haul transmissions. In addition, a 1.1 dB reduction of the required OSNR and 2.6 dB launch power range extension are observed in the triple-carrier 480 Gb/s Nyquist DP 16-QAM back-to-back and 700 km transmission experiments, respectively. The advantages of the proposed low-complexity MAP scheme make it a preferable impairment mitigation technique for practical Nyquist-WDM systems.

Index Terms: Maximum-a-posteriori-probability detection, pattern-dependent impairment mitigation, coherent optical communication, quadrature amplitude modulation.

1. Introduction

In the past decade, large capacity WDM optical transmission systems have been commercially deployed due to the advances of digital signal processing (DSP), and it is certified that increasing both per channel spectral efficiency (SE), data rate and nonlinearity tolerance can effectively reduce cost per bit and increase transmission efficiency [1]–[3]. Moving forward to the next generation network, to satisfy the ever-increasing capacity demands raised by Internet services such as HD video streaming, virtual reality, cloud computing, automatic drive, 5G and so on emerging applications, optical transport with higher bit rates and greater network resource utilizations has considered as

an inevitable step as the next generation WDM transmission [4]–[6]. Accordingly, single-carrier (SC) Nyquist pulse filtered dual-polarization (DP) multilevel quadrature amplitude modulation (m-QAM), i.e., the super channels composed of several subcarriers, together with digital coherent detection and higher data rates, represents an attractive solution to achieve high bite rate and high SE [7], [8]. In addition, with the help of increased launch power, higher signal power can be obtained for satisfying the optical signal-to-noise ratio (OSNR) requirement that enables long-haul reliable transmission. Note that although orthogonal frequency division multiplexing (OFDM) also can achieve high SE, SC modulation exhibits advantages such as better nonlinearity tolerance and higher laser linewidth tolerance [9].

It is noteworthy that advanced QAM signal is more susceptible to both linear and nonlinear impairments due to the various amplitudes and shorter Euclidean distance. In particular, the tight pre-filtering using low-cost digital FIR filters with imperfect window at a transmitter helps to tighten channel spacing for achieving high SE, but it inevitably causes severe inter-symbol-interference (ISI) for a subcarrier in Nyquist multi-carrier modulation system, as the pre-filtered QAM signal broadens in time domain and is with memory because adjacent symbols exchange energy through ISI [10]. In addition, although higher launch power directly contributes to adequate OSNR, it also induces fiber nonlinear effects including intra-channel nonlinearities coming from self-phase modulation (SPM) and inter-carrier nonlinearities originating from cross-phase modulation (XPM), and four-wave mixing (FWM) between subcarriers in a WDM system [11], [12]. The fiber nonlinear effects, especially the SPM in Nyquist WDM systems, generate nonlinear phase impairments and thereby lead to serious performance penalty. Therefore, simultaneous mitigation of tight pre-filtering and fiber nonlinearity impairments is of uppermost priority for a Nyquist WDM long-haul transmission. Thanks to that the full optical field information is preserved and available, digital coherent detection offers a cost-effective way to mitigate such impairments in the electrical domain using advanced DSP.

Various approaches have been proposed to compensate/mitigate above impairments using Tx- and/or Rx-side DSP. The current mainstream techniques for fiber nonlinear effect compensation include digital back-propagation (DBP) algorithms [13]–[16], time/frequency-domain Volterra series-based equalizers [17]–[19], machine learning-based techniques [20]–[22], nonlinear Fourier transform (NFT) [23], maximum likelihood sequence estimation (MLSE) [24], [25], and regular perturbation-based methods [26]. However, most of the methods mentioned above require detailed knowledge of the transmitted signals and generally groan under the intolerable burden of massive CC, thereby hindering their practical application. On the other hand, considering that Nyquist filtering and fiber nonlinear effects both make the transmitted signal exhibit a pattern-dependent distortion with memory, another more attractive approach with relatively lower CC, namely maximum-a-posteriori probability (MAP) detection, also has been presented for mitigating multiple linear and nonlinear impairments [27]–[32]. The MAP detector can perform parallel processing for all sub-carriers simultaneously. It typically captures the distortion-degraded signals during the training phase and uses this knowledge to build look-up tables (LUTs). Then an efficient detection of the transmitted symbol is implemented by finding the LUT entry that enables the received signal pattern with maximum a posteriori probability. However, to the best of our knowledge, the posteriori probability in MAP detection is still determined by calculating the conventional Euclidean distance (ED) between the pending pattern and every LUT entry, thereby requiring MN entries in N-symbol LUT for M-QAM signals which causes exponential-growth CC due to huge multiplications of the ED calculation.

In this paper, facing the challenge that imperfect tight filtering and fiber nonlinearity impairments are major limiting factors of system performance, an innovative multiplier-free MAP detection, modified form our recently reported scheme [33] with further reduced CC, is proposed and investigated in simulations and experiments. Based on the technique of approximate calculation of the ED, the CC of the MAP detector could be significantly reduced while the competitive performance of pattern-dependent impairments mitigation is still maintained. Comprehensive simulation results demonstrate that the MAP scheme could effectively mitigate the fiber nonlinearity and Nyquist filtering impairments with much lower CC. In addition, the triple-carrier 480 Gb/s Nyquist DP-16QAM

is experimentally carried out to investigate the performance of the scheme in back-to-back and 700 km transmissions, respectively. The remainder of this paper is as follows. Principle explanations as well as CC analyses of the multiplier-free MAP detection are presented in Section 2. Then Section 3 gives comprehensive numerical simulation results and discussions. Section 4 shows the experimental setup and discusses the results of a triple-carrier 480 Gb/s Nyquist DP-16QAM coherent system. Finally, the conclusion of the paper is drawn in Section 5.

2. Scheme Principle

2.1 Principle of MAP Detection

Typically, the MAP detection is performed after constellation recovery to mitigate the pattern-dependent impairments induced by tight filtering and fiber nonlinear effects over each N (N is the MAP memory length or the length of pattern) consecutive symbols.

Here we refer to the best detecting principle to illustrate the principle of MAP detection. Using Bayesian rules, the posterior probability $p(s_i|R)$ can be expressed as

$$P(s_i|R) = \frac{p(R|s_i)p(s_i)}{p(R)} \qquad (i = 1, 2, \ldots, M^N) \tag{1}$$

Where $p(R|s_i)$ is the conditional probability density of the received signal under the condition of the s_i training pattern in the table, $p(s_i)$ is the prior probability of the value of the s_i training pattern, R includes N received samples, $p(R)$ is the distribution of the received samples, and M is the order of M-QAM. According to the Eq. (1), when s_i satisfies the uniform distribution, the maximum of $p(R|s_i)$ means the maximum posterior probability. Therefore, the signal decision criterion can be expressed as

$$\hat{R} = \arg\max_{i\in[1,M^N]} (p(R|s_i)) \tag{2}$$

Where the *argmax* is the operation to find the maximum $p(R|s_i)$, and $\hat{R}$ is the detection output. Assuming that the noise obeys normal distribution and the variables s_i are statistically independent, because the relative position of the magnitude of the value in the likelihood function after the logarithm is not changed, we can take the logarithm of the Eq. (2) as follows.

$$\begin{aligned}\hat{R} &= \arg\max_{s_i\in(M^N)} (\ln p(R|s_i)) \\ &= \arg\max_{i\in[1,M^N]} \left(\ln\left(\frac{1}{\sqrt{\pi N_0}}\exp\left(-\frac{1}{N_0}\sum_{k=1}^{N}|R_k - s_{ik}|^2\right)\right)\right) \\ &= \arg\min_{i\in[1,M^N]} \left(\sum_{k=1}^{N}|R_k - s_{ik}|^2\right) = \arg\min_{i\in[1,M^N]} \left(\sum_{k=1}^{N}|D_{ik}|^2\right)\end{aligned} \tag{3}$$

Where R_k is the kth samples of the received N-symbol pattern, s_{ik} is the kth samples of the ith training pattern, N_0 represents the variance of the noise, and D_{ik} denotes the vector of the difference between the kth symbol of a pending pattern to the corresponding symbol of the ith pattern of LUT. Obviously, the final decision of the MAP detection is determined by finding a LUT pattern that has the minimum Euclidean distance to the current received pattern.

Fig. 1 shows an example of 3-symbol LUT entries of 16-QAM built by averaging the received distorted signals 50 times. At the beginning of MAP detection, a preset training sequence is transmitted when the pattern-dependent impairments exist in system. Initially the LUT entries are all zero. The received samples are fed into a training processor, which arranges the received distorted samples into N-symbol pattern-dependent sets (associated with LUT entries) based on the corresponding original data in a one-sample sliding window. Next, all N-symbol patterns in each set are averaged, thereby reducing the effect of zero mean noise on each set. The averaged sets are stored in a

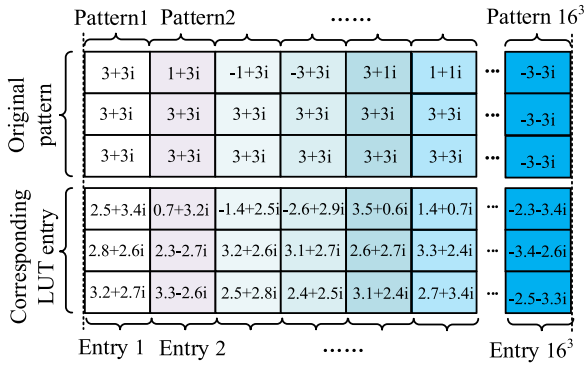

Fig. 1. The example of 3-symbol LUT entries built by averaging the received distorted signals 50 times.

memory as the LUT entry and indexed by the original symbol pattern. It is worth noting that the table can be dynamically updated in a new operation to achieve adaptive mitigation of time-varying impairments in transmission.

After the LUT is created in "training phase", the received data samples are similarly arranged by a one-sample sliding window, and then performing the MAP detection in which the posteriori probability is calculated based on the ED between the input N-symbol pattern (one sample per symbol) and corresponding LUT entries. For a present N-symbol pattern, the MAP detection result for the center symbol is determined by finding the LUT entry that has the minimum ED. However, because that each symbol in a N-symbol pattern has M different constellations in M-QAM, it requires M^N entries in N-symbol LUT for MAP detection, which cause exponential-growth CC due to huge multiplications of the ED calculation. For example, given that memory length N is three, there are $16^3 = 4096$ LUT entries for 16-QAM signals, thus requiring $3 \times 4096 \times 2$ real multiplications for a center symbol detection. Therefore, it is of significant importance to reduce the CC of MAP detection to realize a low-cost and low power practical implementation. Please note that the MAP detection scheme can work for hard-decision as well as soft-decision, and in this paper it directly outputs the constellation hard-decision result and then performs the direct BER counting using rectilinear decision boundaries.

2.2 Approximate Calculation of the ED

To reduce the CC of massive ED calculations, here an approximate ED calculation method is introduced, based on the fact that the results of absolute operations on cosine and sine functions are very close to those of square operations [34]. As shown in Fig. 2, the comparison between absolute operation and square operation indicates that it could be a good solution using absolute operation of real part and imaging part of the vector to simplify the square operation, as fallows.

$$\begin{cases} \cos^2(\varphi) \approx \left|\cos(\varphi)\right| \\ \sin^2(\varphi) \approx \left|\sin(\varphi)\right| \end{cases} \tag{4}$$

Where $|\cdot|$ stands for taking absolute value. For a vector D_k (the vector of the difference between the kth symbol of a pending pattern and the corresponding symbol in one entry of the LUT), its real part d_I(k) and imaginary parts d_Q(k) can be simply expressed as

$$\begin{cases} d_I(k) = |D(k)| \cos(\theta_k) \\ d_Q(k) = |D(k)| \sin(\theta_k) \end{cases} \tag{5}$$

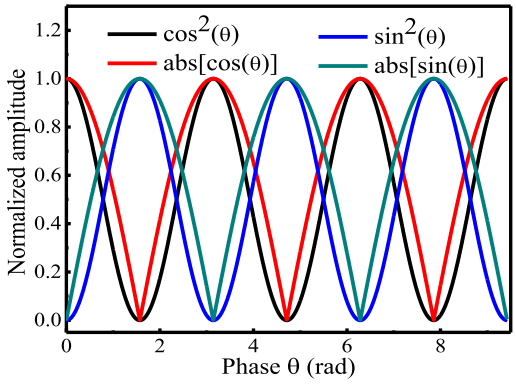

Fig. 2. The comparison between absolute operation and square operation.

Where θ_k is the phase of the vector $D(k)$. Typically, the conventional ED can be calculated as

$$ED = \sum_{k=1}^{N} |D(k)| = \sum_{k=1}^{N} \sqrt{{d_I}^2(k) + {d_Q}^2(k)} \tag{6}$$

Based on the fact that $\cos^2(2\theta_k) + \sin^2(2\theta_k) = 1$, the ED could be rewritten as

$$ED = \sum_{k=1}^{N} |D(k)| \cos^2(2\theta_k) + \sum_{k=1}^{N} |D(k)| \sin^2(2\theta_k) \tag{7}$$

Here, to take the advantage of the relationship between absolute operation and square operation, with the help of the double angle formulas, the cosine term in (7) can be approximately calculated as follows.

$$\begin{aligned}
&\sum_{k=1}^{N} |D(k)| \cos^2(2\theta_k) \approx \sum_{k=1}^{N} \left| D(k) \cdot \cos(2\theta_k) \right| \\
&= \sum_{k=1}^{N} \left| D(k) \cdot \cos^2(\theta_k) - D(k) \cdot \sin^2(\theta_k) \right| \\
&\approx \sum_{k=1}^{N} \left| \left| D(k) \cdot \cos(\theta_k) \right| - \left| D(k) \cdot \sin(\theta_k) \right| \right| \\
&= \sum_{k=1}^{N} \left| |d_I(k)| - \left| d_Q(k) \right| \right|
\end{aligned} \tag{8}$$

Similarly, the sine term in (7) can be approximated as

$$\begin{aligned}
&\sum_{k=1}^{N} |D(k)| \sin^2(2\theta_k) \approx \sum_{k=1}^{N} \left| D(k) \cdot \sin(2\theta_k) \right| \\
&= \sum_{k=1}^{N} \left| D(k) \cdot \left[\sin^2(\theta_k + \pi/4) - \cos^2(\theta_k + \pi/4) \right] \right| \\
&\approx \sum_{k=1}^{N} \left| D(k) \cdot \left[\left| \sin(\theta_k + \pi/4) \right| - \left| \cos(\theta_k + \pi/4) \right| \right] \right|
\end{aligned}$$

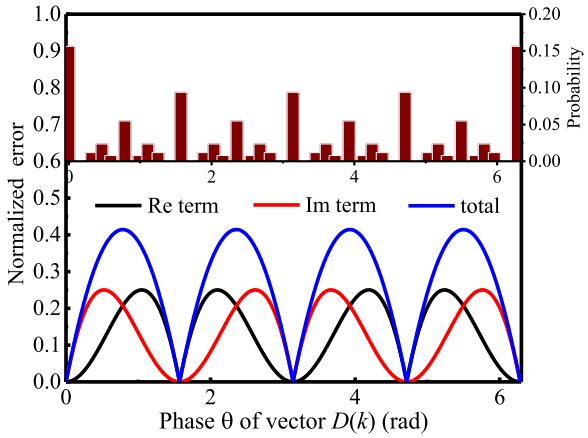

Fig. 3. The approximation error (bottom) and its probability of occurrence (top).

$$= \sqrt{2/2} \cdot \sum_{k=1}^{N} \left| D\ (k) \cdot \left[\left| \cos(\theta_k) + \sin(\theta_k) \right| - \left| \cos(\theta_k) - \sin(\theta_k) \right| \right] \right|$$

$$= \sqrt{2/2} \cdot \sum_{k=1}^{N} \left| \left| d_I\ (k) + d_Q\ (k) \right| - \left| d_I\ (k) - d_Q\ (k) \right| \right| \tag{9}$$

Finally, the ED can be approximately calculated as

$$ED = \sum_{k=1}^{N} \left| |d_I\ (k)| - \left| d_Q\ (k) \right| \right| + \sqrt{2/2} \cdot \sum_{k=1}^{N} \left| \left| d_I\ (k) + d_Q\ (k) \right| - \left| d_I\ (k) - d_Q\ (k) \right| \right| \tag{10}$$

It should be noted that all of the above operations are independent of the modulation format, i.e., the approximate calculation of ED can be applied to systems using any modulation format.

2.3 Approximation Accuracy Evaluation

One can see from the Fig. 2 that for a given phase the accuracy for approximation of square operation with absolute value is not exactly accurate enough, which seems to be too much for estimating the ED for closely spaced signal patterns. Therefore, to further evaluate the proposed method, the accuracy for approximation of square value with absolute value is investigated.

Fig. 3 shows the relationship between the approximation error of vector $D(k)$ and its corresponding probability of occurrence. It can be observed that errors of the real and imaginary parts of the vector $D(k)$ present a periodic law in the range of $0 \sim 2\pi$ respectively, which can be attribute to the symmetry of the QAM constellation. Furthermore, the total error (the sum of the real and imaginary errors) increases first and then decreases in the range of $[0 + k \cdot \mathrm{pi}/2 \sim \mathrm{pi}/2 + k \cdot \mathrm{pi}/2]$, $(k = 0,\ 1,\ 2 \ldots)$, resulting in a maximum value when the phase θ_k of vector D_k equals to $\mathrm{pi}/4 + k \cdot \mathrm{pi}/2$. Besides, the error near $k \cdot \mathrm{pi}/2$ angles is approximately equal to zero. It is worth noting that, as shown in the insert picture, for a single vector $D(k)$ the probability that the total error locates close to its maximum value is about 0.015. Therefore, for a combination of $D(k-1)$, $D(k-1)$ and $D(k+1)$, i.e., a 3-symbol pattern, the probability of occurrence of the maximum approximation error is exactly very small (about 0.015^3 = 3.4E-6) that can be reasonably ignored for estimating the ED. So we

TABLE 1
CC Comparison of 3-Symbol MAP Detections for 16-QAM (M = 16, N = 3)

	real multipliers	square root	real adders	comparators
Conventional MAP	$2N{\cdot}M^N$ (24576)	$N{\cdot}M^N$ (12288)	$N{\cdot}M^N$ (12288)	0
Modified MAP	0	0	$8N{\cdot}M^N$ (98304)	$6N{\cdot}M^N$ (73728)

believe that the approximation accuracy of the proposed method is sufficient for the ED calculation of a 3-symbol pattern.

2.4 Complexity Analysis and Comparison

We compare the CC of the proposed MAP detection scheme with that of the conventional method. For clarity, only real multiplier, square root, real adder and comparator are taken into account, and all complexities are just counted for a received N-symbol pattern in a single polarization. Thus, taking 3-symbol MAP detection of 16-QAM as an example, the complexity computation of the proposed MAP detection scheme is summarized comparatively as follows.

In Eq. (6), calculating the conventional ED for the traditional MAP detection requires 6×4096 real multipliers, 3×4096 taking square root and 3×4096 real adders. By contrast, in the proposed MAP detection, the ED calculation in Eq. (10) requires only 24×4096 real adders and 18×4096 comparators. It is noteworthy that the multiplying $\sqrt{2}/2$ can be approximately replaced by multiplying 7/10, which can be achieved by shift operations and three adders [30]. Note that the complexity of taking absolute values is equal to the complexity of the comparator. In addition, Eq. (8) and Eq. (9) are just used to illustrate the derivation process and have no contribution to the CC.

The CC comparison is summarized in Table 1. In order to compute the CC, based on typical FPGA area costs, real adders are assumed to have unit complexity, comparators have twice complexity as that of real adders, multipliers ten times that of adders, and finally square root 3.8 times that of multipliers, respectively. Therefore, when converting the complexity of all operations into real adders, the CC of the proposed multiplier-free MAP detection is significantly reduced to about 34% compared with conventional scheme.

3. Simulations and Performance Evaluation

To investigate the performance of our proposed MAP detection scheme, we have constructed a triple-carrier 480 Gb/s (20 Gbaud) Nyquist DP 16-QAM BTB and fiber transmission simulation platform, where the subcarrier spacing is 20.5 GHz (slightly larger than the baud rate of each subcarrier, considering the inter-subcarrier crosstalk caused by drifts in the central frequencies of the lasers). The FEC encoding is not applied to the original DP 16-QAM signal in our simulations. Imperfect digital Nyquist pulse shaping is employed by transmitter-side (T_x) DSP to narrow the modulated signal spectrum and thereby enhance the spectral efficiency without using expensive optical filtering. The transmission line consists of multiple spans of 100 km standard single mode fiber (SSMF) with a chromatic dispersion (CD) coefficient of 17 ps/nm/km, a fiber effective area of 80 um^2, a fiber nonlinear index of 2.6e-20 m^2/W and a loss coefficient of 0.2 dB/km. An optical amplifier after each span is used to compensate for the transmission loss. We assume no phase noise (induced by laser linewidth), neither for the transmit laser nor for the LO, is considered here. White Gaussian noise is added in front of the receiver to adjust OSNR. The middle subcarrier is coherently detected and investigated without/with MAP detection. Fig. 4(a) and 4(b) show the DSP blocks at the transmitter and the receiver respectively. Before performing the MAP detection, I/Q imbalance correction, CD compensation, polarization de-multiplexing, frequency offset compensation and carrier phase estimation should be carried out respectively. We first propagate 10^6

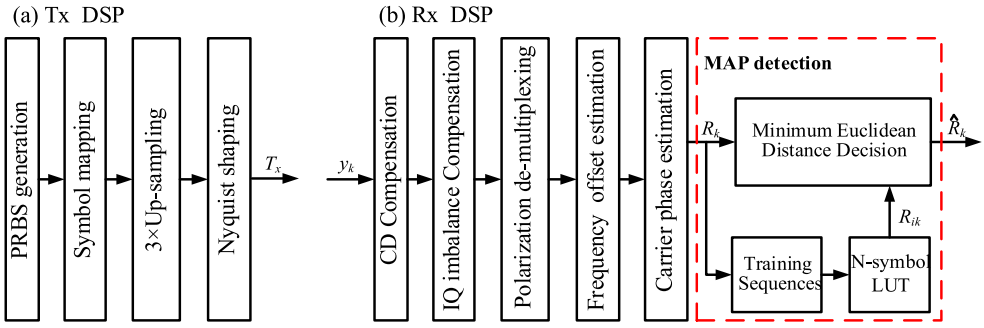

Fig. 4. The DSP blocks at (a) the transmitter and (b) the receiver for DP 16-QAM signals with MAP detection.

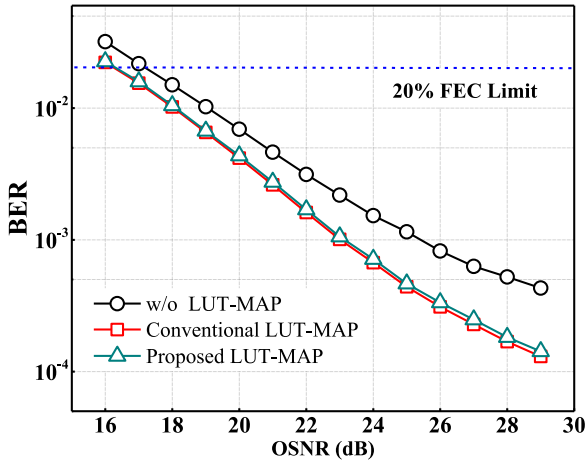

Fig. 5. BER dependence on OSNR in the BTB scenario for the center subcarrier in the triple-carrier 480 Gb/s Nyquist DP 16-QAM system with/without the 3-symbol MAP detections.

symbols in the transmission line for MAP detection training. After building up the table that stores the pattern-dependent impairments, the transmitted symbols are putted into the MAP detector and then carry out BER counting. Please note that once the LUT table has been obtained in the training phase, the subsequent processing of the same condition transmission does not need to be trained again, which means that the spectral efficiency loss caused by the training is almost negligible.

Fig. 5 shows the BTB bit error rate (BER) performance as a function of OSNR of the triple-carrier 480 Gb/s DP-16QAM BTB signal with and without 3-symbol MAP detection. The results show that the modified MAP detection can effectively mitigate the penalty induced by the tight filtering. The conventional MAP detector yields the best OSNR performance and the required OSNR for the soft-decision (SD) forward error correction (FEC) limit at a BER of 2×10^{-2} is reduced by about 1.5 dB for both MAP detectors. Furthermore, as the OSNR increases, the performance improvement using the MAP detections becomes more significant. Note that the CC reduction for the modified multiplier-free MAP detection causes a negligible penalty in required OSNR compared to the conventional MAP. It is noteworthy that a larger MAP memory length is beneficial to obtaining accurate pattern distortion information. However, a 5-symbol MAP detection shows little performance improvement compare with the 3-symbol MAP in our previous investigations, and the LUT in 5-symbol MAP detection even has 16^5 patterns and requires about 2×10^7 symbols used for training sequences, which causes not only unacceptable spectral efficiency loss but also the computational complexity to increase thousands of times. Therefore, considering the trade-off between

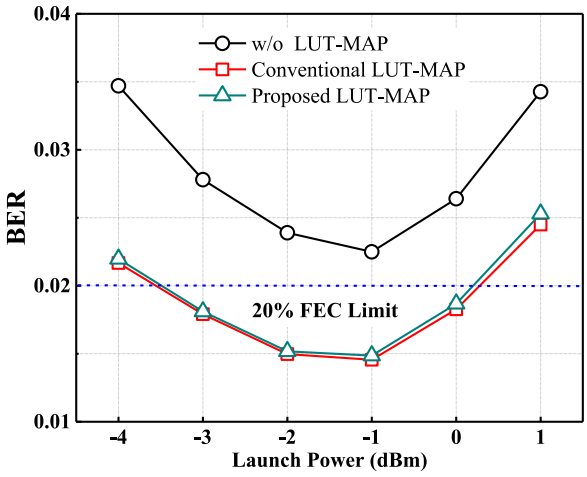

Fig. 6. BER dependence on launch power in 1500 km transmission for the center subcarrier in the triple-carrier 480 Gb/s Nyquist DP 16-QAM system with/without the 3-symbol MAP detections.

the impairment mitigation performance and computational complexity, the MAP memory length of 3 is employed for all measurements in this paper.

For transmission over 1500 km of single-mode fiber, the BER dependencies on launch power are illustrated in Fig. 6 with and without the two 3-symbol MAP detectors. Note that without MAP detection, the BER curve is above the FEC threshold of 2×10^{-2}. By contrast, with the enhancement of MAP detection, the launch power ranges for a BER below the FEC threshold of BER $= 2 \times 10^{2}$ are 3.8 dB and 3.6 dB for the conventional MAP and modified MAP detector, respectively. Compared to the conventional MAP, the launch power range is about 0.2 dB smaller than the proposed MAP with much lower CC, this is mainly attributed to the approximation calculation of the ED. Please note that tight filtering impairments and fiber nonlinearities exist at same time in the system. When launch power is less than optimum launch power (linear regime), optical amplifier noise and tight filtering impairments dominate BER performance, while it is fiber nonlinearity that dominate BER performance when launch power is larger than optimum value (nonlinear regime). The results show that the gains of MAP detections in the linear and nonlinear regimes are nearly equivalent, which demonstrate that the proposed MAP could mitigate the tight filtering and fiber nonlinearity impairments simultaneously.

Fig. 7 indicates the BER dependence on fiber length for the 480 Gb/s DP-16QAM signal with an optimum launch power of -1 dBm without and with the conventional and proposed multiplier-free MAP detections. The 3-symbol modified MAP detector almost has the same performance compared to conventional MAP detection at the FEC threshold. The improved performance of the two MAP detections allows transmission over 1800 km at the FEC threshold of BER $= 2 \times 10^{2}$, while it is only 1400 km without MAP detection, i.e., achieves an effective pattern-dependent impairments mitigation and increases the achievable transmission distance by about 28%.

Nyquist-WDM systems can help to tighten channel spacing for achieving high SE, but it is inherently susceptible to carrier frequency drift. As shown in Fig. 8, frequency drift will decrease channel bandwidth utilization and further deteriorate system performance. Besides, the actual channel center in a ROADM optical network also may vary over time due to the impact of environmental conditions, and such a ROADM passband variation may further decrease channel bandwidth utilization. Therefore, as shown in Fig. 9, the effect of different subcarrier frequency drifts is investigated in the 1500 km transmission with the optimum launch power of -1 dBm. It can be observed that the BER rises steeply with the growing frequency drift. Fortunately, the result shows that with either MAP detection it always can achieve a BER below the FEC threshold of 2×10^{-2} with the frequency drifts range of $-0.5 \sim 0.5$ GHz.

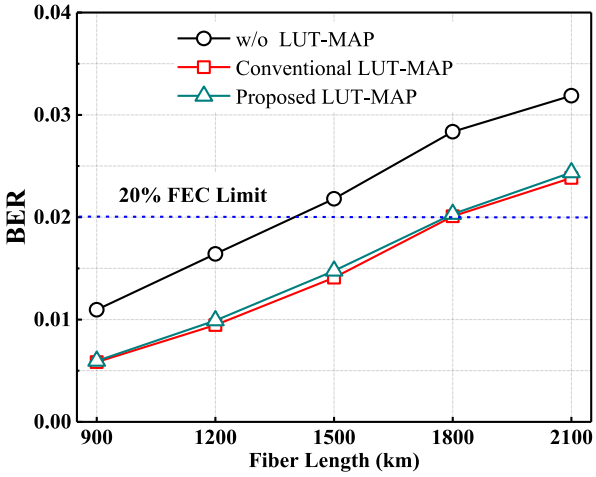

Fig. 7. BER on fiber length for the center subcarrier in the triple-carrier 480 Gb/s Nyquist DP 16-QAM system with/without the 3-symbol MAP detections.

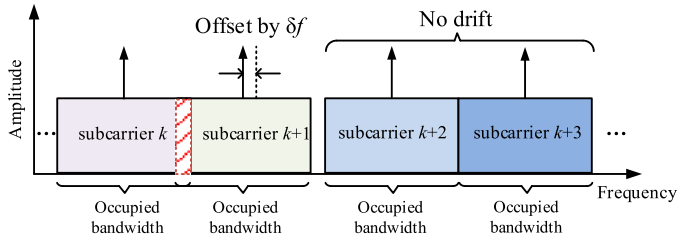

Fig. 8. Impact of carrier frequency drift on the usable channel bandwidth.

4. Experiment Setup and Results

To further investigate the performance of the proposed MAP detection, as shown in Fig. 10, the BTB and 700km transmission experiments for the triple-carrier 480Gb/s Nyquist DP 16-QAM with a subcarrier spacing of 20.5 GHz have been carried out. At the transmitter, $2^{21}-1$ PRBS is used to generate 4-level Gray mapped signals. Note that the FEC encoding is not employed in the experiment. The Nyquist pulse shaping is realized in the digital domain by FIR filters. Threefold oversampling is performed for providing 20 Gbaud signals. The four signals are sent into an arbitrary waveform generator (AWG) with four synchronized 60 GSa/s DACs. The AWG output differential signals drive two DP I/Q modulators, one for subcarrier 1 and 3 and the other for the central subcarrier 2. Then three subcarriers are combined by a coupler and launched into a re-circulating transmission fiber loop, which consists of optical couplers, loop switches, 10 spans of 70 km conventional SMF with an attenuation of 0.17 dB/km and CD of 17 ps/nm/km, and an EDFA. Here no inline or pre/post-optical CD compensation was used in the experiment. At the receiver, before detected by the coherent receiver, the Nyquist DP 16-QAM signal is applied to a programmable optical filter (POF) with 0.16 nm 3-dB bandwidth and 1 GHz resolution to choose the center subcarrier (i.e., demultiplex the channels). The OSNR is measured by an optical spectrum analyzer (OSA) with 0.1 nm noise reference bandwidth. The ECL local oscillator has a typical linewidth of 50 kHz. The optical signal is sampled by a 40 GS/s real-time oscilloscope (3-dB bandwidth 16.8 GHz). In the offline DSP, I/Q imbalance recovery, CD compensation and polarization de-multiplexing (constant modulus algorithm (CMA) for pre-convergence then switching to radius-directed equalization (RDE)) are carried out for two samples per symbol signals respectively. Then frequency offset estimation [35] and carrier phase estimation [36] are performed. After recovering

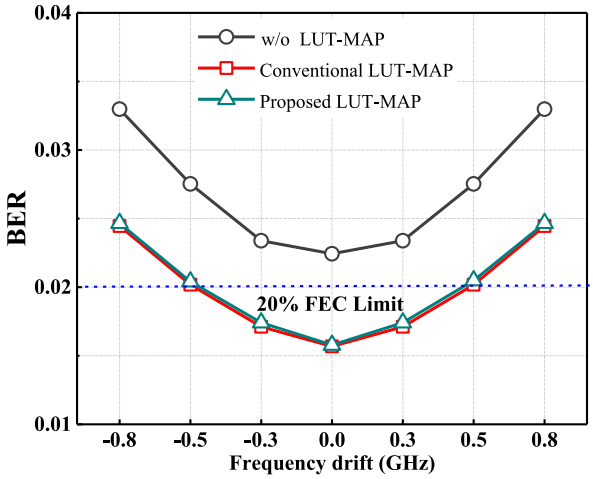

Fig. 9. BER on frequency drift for the center subcarrier in the triple-carrier 480 Gb/s Nyquist DP 16-QAM system with/without the 3-symbol MAP detections.

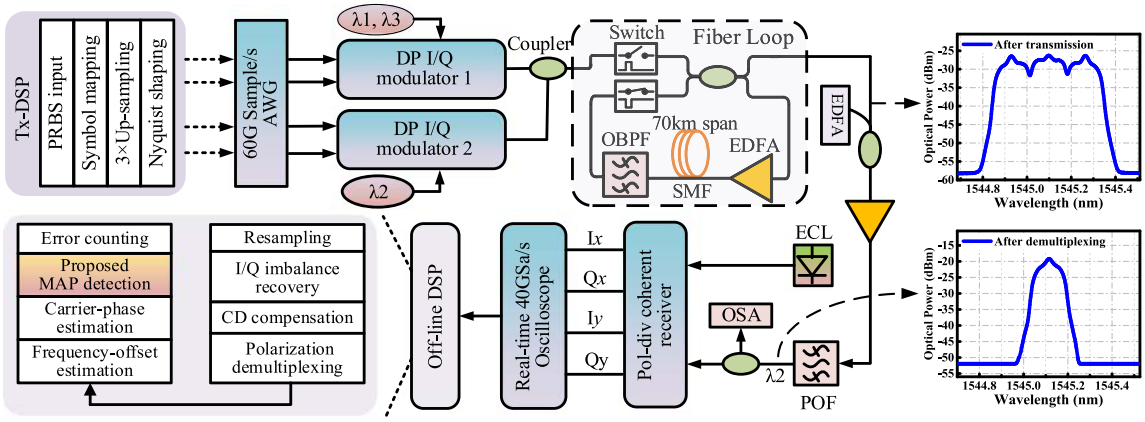

Fig. 10. Experimental setup for back-to-back and transmission measurements. (EDFA: erbium-doped fiber amplifier, SMF: single mode fiber, OBPF: optical band pass filter, POF: programmable optical filter, ECL: external cavity laser, OSA: optical spectrum analyzer.)

the signal constellation, the MAP detection is subsequently carried out. Note that we process more than 1M samples for each measurement point. The MAP detector is trained and the LUT is generated by using the first 600k samples. The LUT is then applied to the later 400k samples in both MAP detections. As described in the simulation, once the LUT table has been obtained in the training phase, it does not need to be trained again for the next processing, thereby the SE loss caused by the training is negligible. Fig. 11 shows the BTB electrical spectrum at the transmitter and receiver as well as the recovered constellations of X/Y-polarization for the center subcarrier in the DP 16-QAM experiment.

Fig. 12 shows the BER dependence on OSNR for the triple-carrier 480 Gb/s Nyquist DP 16-QAM BTB system. The conventional MAP detector maintains the best OSNR performance which is consistent with the simulation results. The required OSNR for the SD-FEC limit at a BER $= 2 \times 10^{2}$ is about 19.1 dB by using 3-symbol modified MAP detection, which shows comparable performance to conventional MAP detection, as that 1.1 dB reduction of the required OSNR is obtained. The results show that the modified MAP detection can effectively mitigate the penalty induced by the tight filtering. Similar to the simulation results, the MAP benefit is OSNR dependent. At lower OSNR, the signal is noise dominated and the MAP benefit is relatively small.

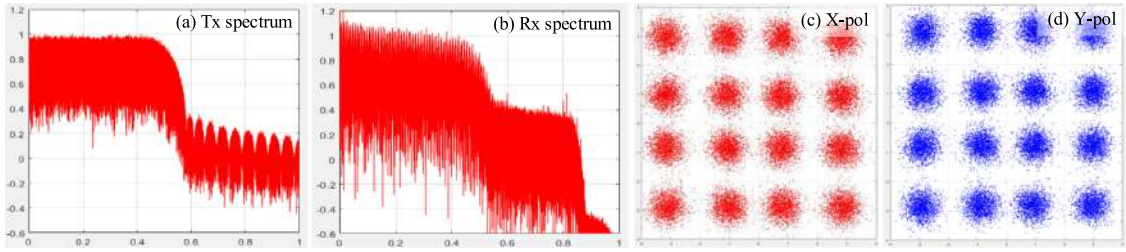

Fig. 11. The BTB electrical spectrum at (a) the transmitter and (b) the receiver, and the recovered constellations of (c) X- and (d) Y-polarization for the 20 Gbuad center subcarrier in the DP 16-QAM experiment.

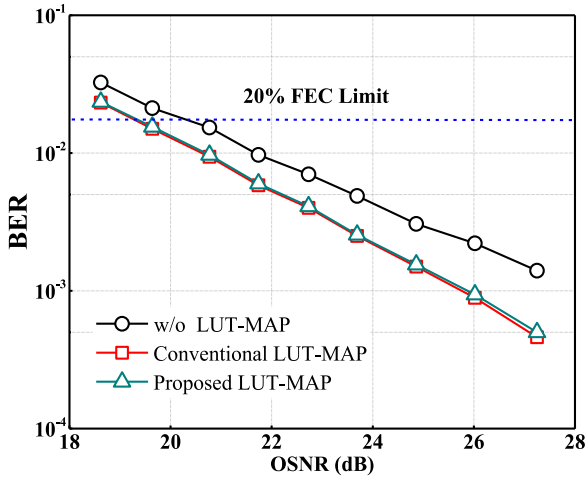

Fig. 12. BER as a function of OSNR in the BTB scenario for the triple-carrier 480 Gb/s Nyquist DP 16-QAM coherent systems with and without MAP detections.

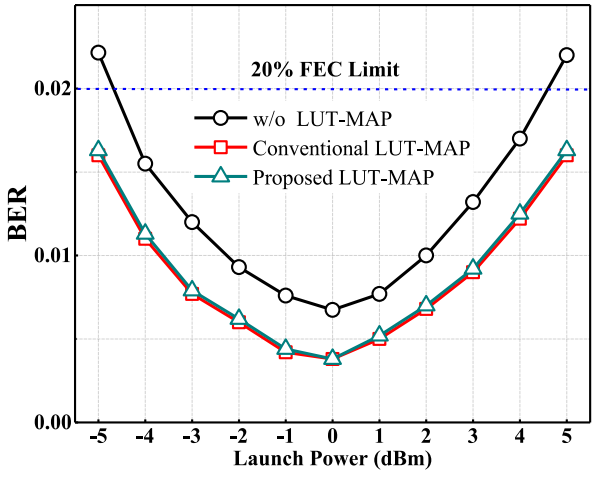

Fig. 13. BER dependence on launch power in 700 km transmission for the triple-carrier 480 Gb/s Nyquist DP 16-QAM coherent systems with and without MAP detections.

The BER dependency on optical launch power for transmission over 700 km SMF in the experiment is illustrated in Fig. 13. It is shown that applying MAP detection on the received signals with the same MAP memory length of 3, the BER curve always below the FEC threshold of 2×10^{-2} in the launch power region of $-5\sim5$ dBm. The result shows that with MAP detection the launch power range of $-2.3\sim2$ dBm has been enlarged to the range of $-3.7\sim3.2$ dBm, resulting in 2.6 dB launch power range extension for achieving a BER below 1×10^{-2}. The two MAP detections achieve almost the same performance on tight filtering and fiber nonlinearity impairments mitigation in long-haul transmissions. In addition, consistent with the simulation results presented in Fig. 6, the optimum launch power keeps unchanged, due to that MAP detections provide almost the same gains on tight filtering impairment mitigation in the linear regime and fiber nonlinearity mitigation in the nonlinear regime.

5. Conclusion

In this paper, facing the challenge that tight filtering and fiber nonlinearity impairments are major limiting factors of Nyquist-WDM system performance, an innovative multiplier-free MAP detection scheme has been proposed and investigated. Based on the technique of the approximate ED calculation, pattern-dependent impairments induced by the tight filtering and fiber nonlinearity can be mitigated simultaneously and effectively, while the CC is drastically reduced to 34% by contrast with conventional MAP, thereby enabling its practical application with low cost and power consumption. Comprehensive simulation results of the triple-carrier DP 16-QAM Nyquist-WDM system demonstrate that the proposed MAP scheme could effectively mitigate the impairments with much lower CC, as that the achievable transmission distance is increased by about 28%, the required OSNR for the FEC limit at a BER of 2×10^{-2} is reduced by about 1.5 dB, and the frequency drifts tolerance can be extended to the range of $-0.5\sim0.5$ GHz. In addition, the performance has been experimentally investigated in triple-carrier 480 Gb/s Nyquist DP 16-QAM BTB and 700 km transmission scenarios respectively, where 1.1 dB reduction of the required OSNR and 2.6 dB launch power range extension are achieved. The advantages of the proposed low-complexity MAP scheme make it a preferable alternative to powerful impairments mitigation for *m*-QAM signals in the practical Nyquist WDM systems.

References

[1] P. J. Winzer, D. T. Neilson, and A. R. Chraplyvy, "Fiber-optic transmission and networking: The previous 20 and the next 20 years," *Opt. Exp.*, vol. 26, no. 8, pp. 24190–24239, 2018.

[2] A. Lau *et al.*, "Advanced DSP techniques enabling high spectral efficiency and flexible transmissions: Toward elastic optical networks," *IEEE Signal Process. Mag.*, vol. 31, no. 2, pp. 82–92, Mar. 2014.

[3] Y. Ji, J. Zhang, X. Wang, and H. Yu, "Towards converged, collaborative and co-automatic (3C) optical networks," *Sci. China Inf. Sci.*, vol. 61, 2018, Art. no. 121301.

[4] Z. Zheng *et al.*, "Fiber nonlinearity mitigation in 32-gbaud 16QAM Nyquist-WDM systems," *J. Lightw. Technol.*, vol. 34, no. 9, pp. 2182–2187, May 2016.

[5] X. Zhou and L. Nelson, "Advanced DSP for 400 Gb/s and beyond optical networks," *J. Lightw. Technol.*, vol. 32, no. 16, pp. 2716–2725, Aug. 2014.

[6] A. Amari, O. A. Dobre, R. Venkatesan, O. S. S. Kumar, P. Ciblat, and Y. Jaouën, "A survey on fiber nonlinearity compensation for 400 Gb/s and beyond optical communication systems," *IEEE Commun. Surv. Tut.*, vol. 19, no. 4, pp. 3097–3113, Oct.–Dec. 2017.

[7] Y. Loussouarn, E. Pincemin, M. Song, S. Gauthier, Y. Chen, and Z. Shengqian, "400 Gbps real-time coherent Nyquist-WDM DP-16QAM transmission over legacy G.652 or G.655 fibre infrastructure with 2 dB margins," in *Proc. Opt. Fiber Commun. Conf.*, 2015, Paper W3E.3.

[8] F. P. Guiomar *et al.*, "Multicarrier digital backpropagation for 400G optical superchannels," *J. Lightw. Technol.*, vol. 34, no. 8, pp. 1896–1907, Apr. 2016.

[9] R. Schmogrow *et al.*, "Real-time Nyquist pulse generation beyond 100 Gbit/s and its relation to OFDM," *Opt. Exp.*, vol. 20, no. 1, pp. 317–337, Dec. 2012.

[10] J. Zhang, J. Yu, and H. Chien, "16 Tb/s (4×400G) unrepeatered transmission over 205-km SSMF using 65-GBaud PDM-16QAM with joint LUT pre-distortion and post DBP nonlinearity compensation," in *Proc. Opt. Fiber Commun. Conf.*, 2017, Paper Th2A51.

[11] R. Maher *et al.*, "Linear and nonlinear impairment mitigation in a Nyquist spaced DP-16QAM WDM transmission system with full-field DBP," in *Proc. Eur. Conf. Opt. Commun.*, 2014, Paper P.5.10.

[12] D. Rafique, "Fiber nonlinearity compensation: Commercial applications and complexity analysis," *J. Lightw. Technol.*, vol. 34, no. 2, pp. 544–553, Jan. 2016.
[13] T. Xu *et al.*, "Digital nonlinearity compensation in high-capacity optical communication systems considering signal spectral broadening effect," *Sci. Rep.*, vol. 7, no. 1, 2017, Paper 12986.
[14] T. Eduardo and R. Stojan, "Overcoming Kerr-induced capacity limit in optical fiber transmission," *Science*, vol. 348, pp. 1445–1448, 2015.
[15] R. Maher *et al.*, "Spectrally shaped DP-16QAM super-channel transmission with multi-channel digital back-propagation," *Sci. Rep.*, vol. 5, no. 8214, pp. 1–8, 2015.
[16] J. Zhang, J. Yu, and H. Chien, "Linear and nonlinear compensation for 8-QAM SC-400G long-haul transmission systems," *J. Lightw. Technol.*, vol. 36, no. 2, pp. 495–500, Jan. 2018.
[17] F. P. Guiomar, J. D. Reis, A. Carena, G. Bosco, A. L. Teixeira, and A. N. Pinto, "Experimental demonstration of a frequency-domain Volterra series nonlinear equalizer in polarization-multiplexed transmission," *Opt. Exp.*, vol. 21, no. 1, pp. 276–288, 2013.
[18] A. Amari, O. A. Dobre, and R. Venkatesan, "Fifth-order Volterra series based nonlinear equalizer for long-haul high data rate optical fiber communications," in *Proc. IEEE Int. Conf. T ran sp. Opt. Netw.*, Jan. 2017, Paper We.A1.2.
[19] F. P. Guiomar, S. B. Amado, C. S. Martins, and A. N. Pinto, "Time-domain volterra-based digital Backpropagation for coherent optical systems," *J. Lightw. Technol.*, vol. 33, no. 15, pp. 3170–3181, Aug. 2015.
[20] J. Zhang, W. Chen, M. Gao, and G. Shen, "K-means-clustering-based fiber nonlinearity equalization techniques for 64-QAM coherent optical communication system," *Opt. Exp.*, vol. 25, no. 22, pp. 27570–27580, 2017.
[21] D. Wang *et al.*, "Intelligent constellation diagram analyzer using convolutional neural network-based deep learning," *Opt. Exp.*, vol. 25, no. 15, pp. 17150–17166, 2017.
[22] E. Giacoumidis, J. Wei, I. Aldaya, and L. P. Barry, "Exceeding the nonlinear Shannon-limit in coherent optical communications using 3D adaptive machine learning," 2018, arXiv: 1802.09120.
[23] S. T. Le, V. Aref, and H. Buelow, "Nonlinear signal multiplexing for communication beyond the Kerr nonlinearity limit," *Nature Photon.*, vol. 11, no. 9, pp. 570–576, 2017.
[24] O. S. S. Kumar, A. Amari, O. A. Dobre, and R. Venkatesan, "Enhanced regular perturbation-based nonlinearity compensation technique for optical transmission systems," *IEEE Photon. J.*, vol. 11, no. 4, Aug. 2019, Art. no. 7203612.
[25] D. Marsella, M. Secondini, and E. Forestieri, "Maximum likelihood sequence detection for mitigating nonlinear effects," *J. Lightw. Technol.*, vol. 32, no. 5, pp. 908–916, Mar. 2014.
[26] E. da Silva, K. Larsen, and D. Zibar, "Impairment mitigation in superchannels with digital backpropagation and MLSD," *Opt. Exp.*, vol. 23, no. 23, pp. 29493–29501, 2015.
[27] A. Rezania, J. C. Cartledge, A. Bakhshali, and W. Y. Chan, "Compensation schemes for transmitter- and receiver-based pattern-dependent distortion," *IEEE Photon. Technol. Lett.*, vol. 28, no. 22, pp. 2641–2644, Nov. 2016.
[28] J. Huo *et al.*, "Transmitter and receiver DSP for 112 Gbit/s PAM-4 amplifier-less transmissions using 25G-class EML and APD," *Opt. Exp.*, vol. 26, no. 18, pp. 22673–22686, 2018.
[29] A. Rezania and J. C. Cartledge, "Transmission performance of 448 Gb/s single-carrier and 1.2 Tb/s three-carrier superchannel using dual-polarization 16-QAM with fixed LUT based MAP detection," *J. Lightw. Technol.*, vol. 33, no. 23, pp. 4738–4745, Dec. 2015.
[30] Y. Cai, "MAP detection for linear and nonlinear ISI mitigation in long-haul coherent detection systems," in *Proc. IEEE Photon. Soc. Summer Topical Meeting Series*, 2010, pp. 42–43.
[31] A. Bakhshali, W. Y. Chan, A. Rezania, and J. C. Cartledge, "Detection of high baud-rate signals with pattern dependent distortion using hidden Markov modeling," *J. Lightw. Technol.*, vol. 35, no. 13, pp. 2612–2621, Jul. 2017.
[32] S. Zhang *et al.*, "Trans-pacific transmission of quad-carrier 1Tb/s DP-8QAM assisted by LUT-based MAP algorithm," in *Proc. Opt. Fiber Commun. Conf. Exhib.*, 2015, Paper W3G.3.
[33] T. Yang, L. Wang, X. Chen, H. Chen, H. Pan, and X. Luo, "Nyquist filtering and fiber nonlinearity distortions mitigation of three-carrier 480Gb/s DP-16QAM with multiplier-free MAP detection," in *Proc. Opt. Fiber Commun. Conf. Exhib.*, 2019, Paper M1I.1.
[34] J. Han, W. Li, Z. Yuan, Y. Zheng, and Q. Hu, "A simplified implementation method of Mth-power for frequency offset estimation," *IEEE Photon. Technol. Lett.*, vol. 28, no. 12, pp. 1317–1320, Jun. 2016.
[35] X. Zhou, X. Chen, and K. Long, "Wide-range frequency offset estimation algorithm for optical coherent systems using training sequence," *IEEE Photon. Technol. Lett.*, vol. 24, no. 1, pp. 82–84, Jan. 2012.
[36] T. Yang *et al.*, "Linewidth-tolerant and multi-format carrier phase estimation schemes for coherent optical m-QAM flexible transmission systems," *Opt. Exp.*, vol. 26, no. 8, pp. 10599–10615, 2018.